

Multifragment Emission Observed for the Reaction $^{36}\text{Ar} + ^{238}\text{U}$ at $E/A = 35$ MeV

Y. D. Kim, M. B. Tsang, C. K. Gelbke, W. G. Lynch, N. Carlin, Z. Chen, R. Fox, W. G. Gong, T. Murakami, T. K. Nayak, R. M. Ronningen, H. M. Xu, F. Zhu, and W. Bauer
*National Superconducting Cyclotron Laboratory and Department of Physics and Astronomy,
 Michigan State University, East Lansing, Michigan 48824*

L. G. Sobotka, D. Stracener, D. G. Sarantites, Z. Majka,^(a) and V. Abenante
Department of Chemistry, Washington University, St. Louis, Missouri 63130

H. Griffin

Department of Chemistry, University of Michigan, Ann Arbor, Michigan 48109
 (Received 24 January 1989)

The dependence of multifragment-emission processes upon linear momentum transfer to the target residue is determined for ^{36}Ar -induced reactions on ^{238}U at $E/A = 35$ MeV. Significantly more intermediate-mass fragments are emitted in central collisions. Multiplicity distributions for intermediate-mass fragments emitted behind the grazing angle resemble Poisson distributions and are consistent with a stochastic production process. Exit channels with up to five intermediate-mass fragments and two fission fragments were observed.

PACS numbers: 25.70.Np

During the expansion stage of heavy-ion collision, regions of the excited and expanding system may become adiabatically unstable,¹ resulting in density fluctuations which lead to a multifragment disintegration¹⁻⁴ and which could provide information about the equation of state and liquid-gas phase transition of dilute nuclear matter.²⁻⁹ While multifragment emission of intermediate-mass fragments (IMF's, $3 \leq Z \leq 20$) has been clearly identified¹⁰⁻¹³ in nucleus-nucleus collisions at high energies ($E \geq 3$ GeV) the extent of this process at lower energies has not been clearly established. Dynamical calculations suggest that fast multifragmentation processes may occur in intermediate-energy heavy-ion collisions,^{4,14-17} and some multifragment decay processes have been observed.¹⁸⁻²¹

The IMF angular distributions at lower energies are strongly forward peaked,^{18,22,23} consistent with a fast,¹⁸ perhaps multifragment, breakup at forward angles. IMF's emitted to forward angles have been described by nonequilibrium statistical breakup models²² or as the projectilelike residues of a binary deeply inelastic collision.²⁴ Emission at backward angles ($\theta_{\text{c.m.}} \geq 120^\circ$) has been described alternatively by the multifragment²⁵ or binary^{22,26-30} decay of equilibrated reaction residues. To clarify the relative importance of single- and multifragment-emission mechanisms, we have measured, with a large-solid-angle charged-particle detection system,³¹ the IMF multiplicity distributions for fragments emitted beyond the grazing angle in ^{36}Ar -induced reactions on ^{238}U at $E/A = 35$ MeV. To discriminate between fusionlike central and less violent peripheral collisions, the IMF multiplicity distributions were measured in coincidence with two fission fragments from the decay of the associated heavy reaction residues. For IMF's emit-

ted beyond the grazing angle, the relative probabilities for the different IMF multiplicities can be described by Poisson probability distributions suggesting a stochastic IMF production mechanism.

In the experiment, a $^{238}\text{U}\text{F}_4$ target of $400\text{-}\mu\text{g}/\text{cm}^2$ areal density was bombarded by a 1260-MeV ^{36}Ar beam from the K500 cyclotron at Michigan State University. Charged particles were detected with 96 phoswich detectors of the Dwarf-Ball-Wall array developed at Washington University.³¹ Each phoswich detector consisted of a thin fast plastic scintillator foil followed by a thick CsI(Tl) scintillator, with 200- μm plastic scintillation foils and 20-mm CsI(Tl) scintillators at the forward angles, reducing to 40- μm foils and 4-mm CsI(Tl) scintillators at the backward angles. To suppress secondary electrons and x rays, the Dwarf-Ball detectors (located at $\theta \gtrsim 35^\circ$) and Dwarf-Wall detectors (located at $12^\circ \lesssim \theta \lesssim 35^\circ$) were covered by 5-mg/cm²-thick Au foils and 10-mg/cm²-thick Ta foils, respectively. The most forward detectors at $\theta \lesssim 12^\circ$, covering the grazing angle, were shielded by 1-g/cm² Pb absorbers to stop elastically scattered projectiles. These absorbers also stopped IMF's, but allowed the detection of energetic light particles. For light particles, the detection array provided an angular coverage corresponding to about 85% of 4π . For heavy fragments, the coverage was reduced to about 78% of 4π ; about 1% of the loss in coverage is due to the Pb absorbers with additional losses due to poor elemental resolution for detectors located at $\theta \gtrsim 150^\circ$.

Particle identification was achieved by integrating the photomultiplier anode current over three different time gates. This information was combined to obtain the energy of the detected particle as well as elemental identification up to about $Z \approx 6$ and isotopic identifica-

tion for light particles ($Z \leq 2$) stopped in the CsI scintillators. Fission fragments were detected with two X-Y position-sensitive parallel-plate multiwire detectors³² covering angular ranges of $\theta_1 = 36^\circ - 116^\circ$, and $\theta_2 = -(39^\circ - 89^\circ)$ in the reaction plane. In the off-line analysis, energy thresholds for Dwarf-Ball detectors of 12 and 18 MeV for hydrogen and helium nuclei, respectively, and thresholds for Dwarf-Wall detectors of 20 MeV for both hydrogen and helium were used. All heavier particles which passed through the absorber and scintillator foils were analyzed, corresponding to thresholds of $E/A \approx 6-9$ MeV and $E/A \approx 2-3$ MeV for the Dwarf-Wall and Dwarf-Ball detectors, respectively. Unfortunately, double hits by two α particles caused significant contamination in the $Z=3$ particle-identification gate. Therefore, we only present IMF multiplicity distributions for fragments with $Z \geq 4$. Contributions from random events were negligible for all observables discussed in this Letter.

The solid line in Fig. 1 shows the inclusive folding-angle ($\theta_{ff} = \theta_{f1} + \theta_{f2}$) distribution for fission-fission coincidences.³³ The dashed and dotted-dashed curves show folding-angle distributions gated by the detection of at least one and three intermediate-mass fragments at backward angles ($\theta \gtrsim 35^\circ$) in the Dwarf Ball, $N_{IMF}^{(b)} \geq 1$ and 3, respectively. Distributions gated by $N_{IMF}^{(b)} \geq 1$ and

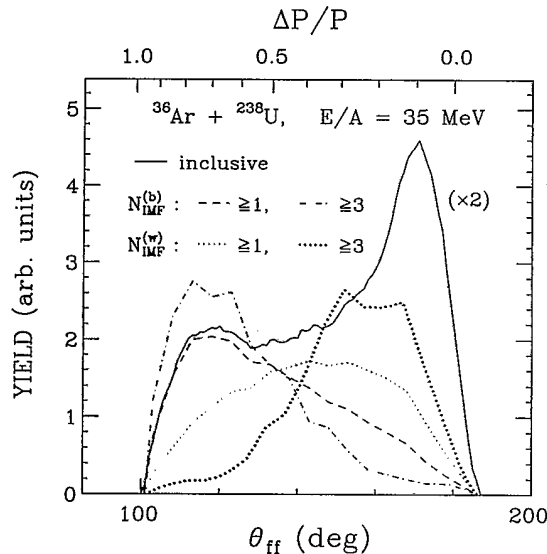


FIG. 1. Folding-angle distributions between coincident fission fragments. The upper scale gives the linear momentum transfer, $\Delta P/P$, in units of the projectile momentum to the heavy reaction residue assuming symmetric fission. The various gating conditions are explained in the text. For comparison, the distributions are normalized to give the same integrated yields, with the inclusive distribution multiplied by an additional factor of 2.0. The measured yields of the inclusive, $N_{IMF}^{(b)} \geq 1$, $N_{IMF}^{(b)} \geq 3$, $N_{IMF}^{(w)} \geq 1$, and $N_{IMF}^{(w)} \geq 3$ spectra are 2.2×10^6 , 3.1×10^5 , 2.6×10^3 , 3.8×10^5 , and 2.1×10^3 counts, respectively.

3 are remarkably similar indicating that single and multifragment emissions to intermediate and large angles can be associated with violent, fusionlike collisions characterized by large linear momentum transfers.^{29,34} The light and heavy dotted curves show distributions gated by the detection of at least one and three intermediate-mass fragments at forward angles ($\theta \lesssim 35^\circ$) in the Dwarf Wall, $N_{IMF}^{(w)} \geq 1$ and 3, respectively. The condition $N_{IMF}^{(w)} \geq 1$ does not select a very specific class of collisions, with contributions from both incomplete fusion reactions and peripheral collisions. The requirement $N_{IMF}^{(w)} \geq 3$, on the other hand, clearly selects more peripheral collisions with smaller linear momentum transfers to the heavy reaction residue.

Figure 2 shows associated charged-particle multiplicities, $N_C = N_{tot} - N_{IMF}^{(gate)}$, where N_{tot} is the total observed charged-particle multiplicity³⁵ (excluding fission fragments) and $N_{IMF}^{(gate)}$ denotes the number of fragments in the gate. The curves are defined as in Fig. 1: The solid line shows the inclusive distribution for fission-fission coincidences; the dashed and dotted-dashed (light and heavy dotted) curves show distributions gated by $N_{IMF}^{(b)} \geq 1$ and 3 ($N_{IMF}^{(w)} \geq 1$ and 3), respectively. A correspondence of collisions with large linear momentum transfers to collisions with large charged-particle multiplicities has been observed previously.^{34,36,37} Consistent with these findings, the observed associated charged-particle multiplicities are large for IMF's emitted at $\theta \gtrsim 35^\circ$ and rather similar for the $N_{IMF}^{(b)} \geq 1$ and 3 gates. The requirement $N_{IMF}^{(w)} \geq 3$ leads to lower mean associated charged-particle multiplicities consistent with a bias towards more peripheral collisions. The different gates discussed in Figs. 1 and 2 clearly select different classes

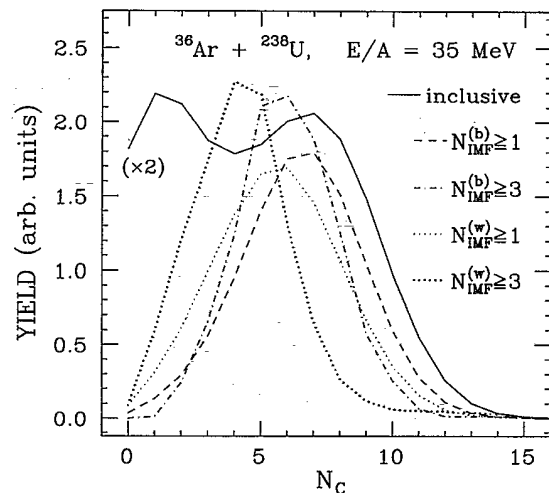


FIG. 2. Associated charged-particle multiplicities, N_C . The various gating conditions are explained in the text. For comparison, the distributions are normalized to give the same integrated yields, with the inclusive distribution multiplied by an additional factor of 2.0.

of collisions reflecting impact-parameter ambiguities which obscure the interpretation of inclusive data. These ambiguities can be removed by suitable choices of reaction filters.

Figure 3 shows probabilities for observed multiplicities, N_{IMF} , of intermediate-mass fragments³⁵ for different gates on folding angle. Open circles correspond to the inclusive distributions for fission-fission coincidences; open squares correspond to small-momentum-transfer collisions gated by $\theta_{\text{ff}} > 160^\circ$ ($\Delta P/P < 0.2$); solid points correspond to large-momentum-transfer collisions gated by $\theta_{\text{ff}} \leq 133^\circ$ ($\Delta P/P \geq 0.5$). Both single and multifragment emissions occur with significantly higher probabilities in central collisions characterized by large linear momentum transfers. (The present experiment cannot address whether even higher multiplicities would be characteristic of collisions which do not lead to fission). Even though most IMF's are produced in events with $N_{\text{IMF}}=1$,²⁴ unit IMF multiplicity does not appear uniquely significant. Instead, the multiplicity distributions decrease monotonically from $N_{\text{IMF}}=0$ and are rather well described by Poisson probability distributions (an example is shown by the solid curve).

Poisson distributions are characteristic of processes which occur with a low and constant probability. Such conditions may prevail for nuclear decays at high excitation energies and with low fragment multiplicities. For example, the statistical weight for fragment emission is small as compared to that for light-particle emission when calculated in a statistical-rate-equation approach,^{27,28,38-40} such as a sequential-evaporation model.^{27,28,40} In this case, deviations from Poisson distribu-

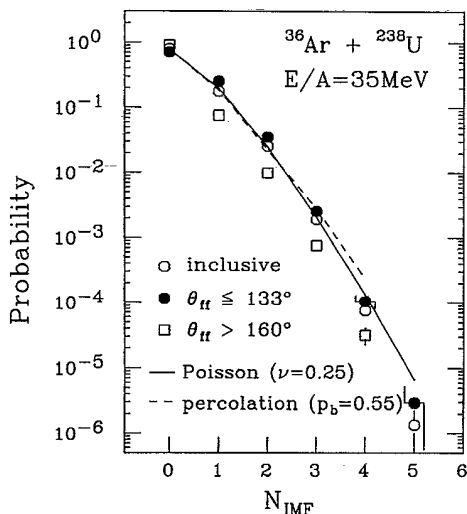


FIG. 3. Probabilities per fission trigger for the detection of single and multiple fragments with $Z \geq 4$. Open circles: no gate on θ_{ff} ; open squares: $\theta_{\text{ff}} > 160^\circ$; solid points: $\theta_{\text{ff}} \leq 133^\circ$. Solid curve: Poisson distribution, $P(N, \nu) = e^{-\nu} \nu^N / N!$, with $\nu = 0.25$; dashed curve: prediction of the percolation model (Refs. 41 and 42) for $p_b = 0.55$.

tions would be expected to occur mainly for high fragment multiplicities or small systems when emission probabilities are affected by energy or mass conservation. To illustrate that Poisson distributions may also be expected in a static theory which encompasses a phase transition, we show in Fig. 3 a distribution predicted by the percolation model.^{41,42} While the IMF detection efficiency of the present experiment is sufficient to reveal the qualitative trends of the multiplicity distributions, the IMF yields below the detection thresholds of the present apparatus would be required to determine the exact shape of the multiplicity distributions and hence, definitive values for the percolation parameter p_b or the average ν of the Poisson distribution. A model-independent correction of the IMF detection efficiency is beyond the scope of the present measurement.

To test the assumption of statistically independent emission, with a reduced sensitivity to the detection inefficiency, we have examined the "charge-correlation function,"

$$C(Z_1, Z_2) = N_0 \left(\sum_{i \neq k} Y_{ik}(Z_1, Z_2) \right) / \left(\sum_{i \neq k} Y_i(Z_1) Y_k(Z_2) \right). \quad (1)$$

Here, $Y_{ik}(Z_1, Z_2)$ denotes the coincidence yield for particles of charge number Z_1 and Z_2 detected in detectors i and k , respectively, and $Y_i(Z)$ denotes the singles yield for particles of charge number Z in detector i . To eliminate peripheral interactions, fission-fragment folding angles were restricted to $\theta_{\text{ff}} \leq 133^\circ$ and at least one intermediate-mass fragment, Z_1 , was required to be detected in the Dwarf Ball ($\theta \geq 35^\circ$). The summations over i and k include all detectors in the Dwarf-Ball and Dwarf-Ball-Wall arrays, respectively. The measured values are listed in Table I. They are constant within about $\pm 10\%$, supporting the assumption of statistically independent emission.

In summary, we established the occurrence of multifragment-emission processes for the $^{36}\text{Ar} + ^{238}\text{U}$ reaction at $E/A = 35$ MeV. Single and multiple emissions of

TABLE I. Charge-correlation function defined in Eq. (1) of the text. Fragments with label Z_1 are detected by the Dwarf Ball (at $\theta \geq 35^\circ$). To simplify comparisons, the correlation function was normalized to one at $Z_1 = Z_2 = 5$. Statistical errors are less than 5%. The Li cross sections contain a (20-25)% contamination from α - α double-hit events, causing corrections which cancel to first order in the correlation function.

$Z_1 \backslash Z_2$	Li	Be	B	C
Li	1.05	0.92	0.97	0.94
Be	1.13	1.01	1.04	1.00
B	1.06	0.91	1.00	0.91
C	1.10	1.01	1.01	0.93

intermediate-mass fragments to large angles ($\theta \geq 35^\circ$) occurs essentially in reactions characterized by large associated charged-particle multiplicities and large linear momentum transfers to the heavy reaction residues. The measured fragment multiplicity distributions are well described by Poisson distributions, and the measured charge-correlation functions are constant within about $\pm 10\%$. Both observations are consistent with a stochastic IMF production process. Final states with only one intermediate-mass fragment in the exit channel represent only one of a family of final states. Future experimental and theoretical investigations should address whether such multifragment emissions are better described by models of nearly instantaneous fragmentation or by models of sequential multistep emissions.

This work was supported in part by the National Science Foundation under Grant No. PHY-86-11210 and by the U.S. Department of Energy under Grants No. DE-FC02-87ER40316 and No. DE-FG02-88ER40406. W.G.L. and L.G.S. acknowledge individual support from the NSF. N.C. is supported by the Fundação de Amparo a Pesquisa do Estado de São Paulo, Brazil.

(a)On leave from Institute of Physics, Jagellonian University, PL-30059, Cracow, Poland.

- ¹G. Bertsch and P. J. Siemens, Phys. Lett. **126B**, 9 (1983).
- ²A. Vicentini *et al.*, Phys. Rev. C **31**, 1783 (1985).
- ³R. J. Lenk and V. R. Pandharipande, Phys. Rev. C **34**, 177 (1986).
- ⁴T. J. Schlagel and V. R. Pandharipande, Phys. Rev. C **36**, 162 (1987).
- ⁵J. E. Finn *et al.*, Phys. Rev. Lett. **49**, 1321 (1982).
- ⁶A. S. Hirsch *et al.*, Phys. Rev. C **29**, 508 (1984).
- ⁷A. D. Panagiotou *et al.*, Phys. Rev. Lett. **52**, 496 (1984).
- ⁸X. Campi, Phys. Lett. B **208**, 351 (1988).
- ⁹W. Bauer, Phys. Rev. C **38**, 1297 (1988).
- ¹⁰J. W. Harris *et al.*, Nucl. Phys. A**471**, 241c (1987).
- ¹¹B. V. Jacak, Nucl. Phys. A**488**, 325c (1988).
- ¹²K. G. R. Doss *et al.*, Phys. Rev. Lett. **59**, 2720 (1987).
- ¹³R. Bougault *et al.*, Nucl. Phys. A**488**, 255c (1988).

- ¹⁴D. H. Boal and J. N. Glosli, Phys. Rev. C **37**, 91 (1988).
- ¹⁵W. Bauer *et al.*, Phys. Rev. Lett. **58**, 863 (1987).
- ¹⁶K. Sneppen *et al.*, Nucl. Phys. A**480**, 342 (1988).
- ¹⁷J. Aichelin *et al.*, Nucl. Phys. A**488**, 437c (1988).
- ¹⁸D. J. Fields *et al.*, Phys. Rev. C **34**, 536 (1986).
- ¹⁹D. Pelte *et al.*, Phys. Rev. C **34**, 1673 (1986).
- ²⁰B. Jakobsson *et al.*, Nucl. Phys. A**488**, 251c (1988).
- ²¹R. Trockel *et al.*, Phys. Rev. C **39**, 729 (1989).
- ²²D. J. Fields *et al.*, Phys. Rev. C **30**, 1912 (1984).
- ²³D. E. Fields *et al.*, Phys. Lett. B **220**, 356 (1989).
- ²⁴B. Borderie *et al.*, Phys. Lett. B **205**, 26 (1988).
- ²⁵D. H. E. Gross, Phys. Lett. B **203**, 26 (1988).
- ²⁶L. G. Sobotka *et al.*, Phys. Rev. Lett. **51**, 2187 (1983).
- ²⁷L. G. Moretto, Nucl. Phys. A**247**, 211 (1975).
- ²⁸W. A. Friedman and W. G. Lynch, Phys. Rev. C **28**, 950 (1983).
- ²⁹M. Fatyga *et al.*, Phys. Rev. Lett. **58**, 2527 (1987).
- ³⁰D. R. Bowman *et al.*, Phys. Lett. B **189**, 282 (1987).
- ³¹D. G. Sarantites *et al.*, Nucl. Instrum. Method Phys. Res., Sect. A **264**, 319 (1988). This paper describes the device equipped with fast-slow plastic phoswich elements; these were replaced by plastic-CsI(Tl) phoswich elements.
- ³²A. Breskin *et al.*, Nucl. Instrum. and Methods Phys. Res. **221**, 363 (1984).
- ³³The folding-angle distributions in Fig. 1 have been corrected for geometrical efficiency but could suffer some distortions from averaging over the rather large but finite solid angles of the fission detectors.
- ³⁴R. Trockel, Ph.D. thesis, University of Heidelberg [Report No. GSI-87-17, 1987 (unpublished)]; U. Lynen *et al.* (private communication).
- ³⁵These "observed multiplicities" (or coincidence folds) represent the number of detected particles per fission trigger. They are smaller than the actual multiplicities of emitted particles due to finite detection thresholds and incomplete solid angle coverage.
- ³⁶M. B. Tsang *et al.*, Phys. Lett. B **220**, 492 (1989).
- ³⁷L. G. Sobotka *et al.*, Washington University report, 1988 (to be published).
- ³⁸C. R. Grant, Phys. Rev. C **34**, 1950 (1986).
- ³⁹D. H. Boal, Phys. Rev. C **28**, 2568 (1983).
- ⁴⁰J. Gomez del Campo *et al.*, Phys. Rev. Lett. **61**, 290 (1988).
- ⁴¹W. Bauer *et al.*, Phys. Lett. **150B**, 53 (1985).
- ⁴²W. Bauer *et al.*, Nucl. Phys. A**452**, 699 (1986).